How does ytterbium chloride interact with DMPC bilayers? A computational and experimental study

Miguel A. Gonzalez,[*a] Hanna M. G. Barriga,[†a] Joanna L. Richens,[‡b] Robert V. Law,[a] Paul O'Shea,[b,c] and Fernando Bresme[*a]

Lanthanide salts have been studied for many years, primarily in Nuclear Magnetic Resonance (NMR) experiments of mixed lipid-protein systems and more recently to study lipid flip-flop in model membrane systems. It is well recognised that lanthanide salts can influence the behaviour of both lipid and protein systems, however a full molecular level description of lipid-lanthanide interactions is still outstanding. Here we present a study of lanthanide-bilayer interactions, using molecular dynamics computer simulations, fluorescence electrostatic potential experiments and Nuclear Magnetic Resonance. Computer simulations reveal the microscopic structure of DMPC lipid bilayers in the presence of Yb^{3+}, and a surprising ability of the membranes to adsorb significant concentrations of Yb^{3+} without disrupting the overall membrane structure. At concentrations commonly used in NMR experiments, Yb^{3+} ions bind strongly to 5 lipids, inducing a small decrease of the area per lipid and a slight increase of the ordering of the aliphatic chains and the bilayer thickness. The area compressibility modulus increases by a factor of two, with respect to the free-salt case, showing that Yb^{3+} ions make the bilayer more rigid. These modifications of the bilayer properties should be taken into account in the interpretation of NMR experiments.

1 Introduction

Lipid membranes play a vital role in the compartmentalisation and regulation of cellular contents, providing a physical outer barrier to the cell and its organelles, whilst still enabling communication with the extracellular environment.[1] The complex mixture of lipids and proteins that form the cellular membrane determine the dynamics and structure of the bilayer. In order to explain the role that lipids play within the cell both in structure and signalling events[1] it is vital to understand the behaviour of lipids within the membrane, and their partitioning between the two leaflets in a bilayer. Model membrane systems provide a unique opportunity to study the behaviour of the lipid bilayer using a bottom up approach. Whilst relating these studies back to the native *in-vivo* membrane can be challenging, the simplification in a model system is ideal for understanding specific interactions which are difficult to decouple in a cellular environment due to the complexity of the cell membrane. There are a plethora of established techniques for studying bilayer-charge interactions in model membrane systems, including solid state NMR and fluorescence based assays which use a membrane incorporated fluorescent probe to measure changes in the surface electrostatic potential. This fluorescence assay has previously been used in model membrane systems to show adsorption of Ca^{2+} ions, study membrane-peptide interactions and insertion and to quantify the effects of mineral oils on the binding of oleic acid.[2,3] In this study, we use these techniques to characterise the adsorption of lanthanide ions onto a DMPC bilayer. Lanthanide ions have applications in clinical research including the treatment of burns, anticoagulants, anti-tumour therapy and imaging studies as well as acting as a tool for fundamental studies on model membrane systems.[4] In order to exploit these applications from both a fundamental and clinical perspective, a more detailed understanding of the lanthanide membrane interaction is necessary.

Lanthanides are also widely used in solid state NMR and have been employed during the past two decades in applications ranging from protein structure elucidation to lipid-protein interactions and lipid flip-flop. In the latter application, lanthanide ions applied externally to extruded phospholipid vesicles are used to distinguish between the signal from the inner and outer lipids of the membrane.[5,6] The difference in signal is attributed to lanthanide induced chemical shifts in the NMR signal from the outer head groups of the vesicle. By monitoring the change in this signal

[a] Department of Chemistry, Imperial College London, SW7 2AZ, London UK

[b] School of Life Sciences, University of Nottingham, Nottingham UK

[c] Faculty of Pharmaceutical Sciences, University of British Columbia, Vancouver, Canada

[*] m.gonzalez12@imperial.ac.uk

[*] fbresme@imperial.ac.uk

[†] hanna.barriga04@imperial.ac.uk

[‡] joanna.Richens@nottingham.ac.uk

over time the intrinsic rate of lipid flip-flop within a model membrane system can be quantified.[7] These NMR experiments rely on the asymmetric addition of lanthanide ions thereby creating and maintaining a gradient of salt ions across the lipid membrane.

The use of salt to perform the NMR experiments raises several questions. One that is relevant to our ongoing work is how the salt influences the bilayer structure, and consequently its dynamic properties, particularly flip-flop rates. A microscopic view on how lanthanides interact with bilayer is still lacking. This fact prevents a full validation of a particular method of detection within an assay. Therefore it is necessary to advance in our understanding on the fundamental behaviour of the lipid bilayer, before results from different approaches can be interpreted reliably. To advance in the solution of this problem, we have performed computer simulations of atomistic lipid bilayers in the presence of ytterbium chloride. Our aim is to provide a microscopic view of the lanthanide-bilayer interactions of Yb^{3+}, using conditions guided by solid state NMR and electrostatic potential fluorescence experiments on DMPC bilayers in the presence of ytterbium and dysprosium salts.

Molecular dynamics simulations offer a unique approach to study the molecular interactions of model membranes systems with surrounding ligands/molecules and ions. Recent developments on computational methods and force fields have expanded the scope of lipid simulations,[8] enabling the modelling of highly complex systems with increased numbers of particles. It has been possible to model multicomponent mixtures consisting of lipids, membrane proteins and steroids,[9] which take us closer to the real composition of cell membranes. The impact of different ions on the membrane structure has also been considered from a computational perspective.[10–24] These simulation studies show that the ions can influence the permeability and the stability of the lipid membrane, *e.g.*, by promoting the formation of pores,[25–31] which can act as transient structures that facilitate flip-flop processes. These observations are relevant to NMR experiments that involve charge imbalance across the vesicle walls, although not necessarily to experiments that involve a concentration imbalance only, such as the ones considered in this work.

The majority of the simulation studies performed thus far have focused on the alkali halide ions ($[Na^+,K^+],Cl^-$), which are commonly present in a physiological environment. However, there is less information available on lanthanides, which are commonly used in NMR experiments. Understanding the interactions of these ions with biological membranes can help to assess the reliability of the NMR experiments in the determination of rare event dynamic processes (flip-flop).

In this work, we have combined experimental and computational approaches to investigate the impact that lanthanide salts have on bilayer membranes. We have focused our study on a DMPC model membrane system, which is widely used in biophysics. Our article is structured as follows. Firstly, we report details on the experimental and molecular dynamics methods employed in our work. A section containing our results for lanthanide:lipid interactions follows. We close our paper with a discussion of our main conclusions regarding the impact of lanthanides on the bilayer structure.

2 Methodology

^{1}H NMR was performed on extruded DMPC (1,2-dimyristoyl-sn-glycero-3-phosphocholine) vesicles and the chemical shift and quenching due to the external addition of lanthanide salts was calculated. These experiments have been explained in detail in the Supplementary Information (SI) and show similar trends and shifts when compared to previous literature investigating phospholipid-lanthanide interactions.[32,33] These experiments formed the basis for the model system around which the computational calculations and additional experimental investigations were designed. Briefly, the model systems comprised of a pure DMPC membrane in excess water with a fixed concentration of either $YbCl_3$ or $DyCl_3$ salt in contact with the outer membrane lipids in the bilayer. A schematic of this is shown in Fig. 1 illustrating the interplay between the simulations and experimental length scales. In addition to the NMR experiments we used a fluorescence based assay in which the DMPC vesicles were labelled with the charge sensitive fluorescence probe[2] inducing an increase in fluorescence when the positive cation is adsorbed onto the membrane. These experiments enabled the calculation of the maximum number of ions associated with each DMPC lipid molecule and a comparison to the computational result. Finally, we performed a protein leakage assay using DMPC vesicles loaded with the pH sensitive dye pyranine to explore the effects of ytterbium salt on membrane permeability and the possible existence of pore formation. Detailed methods and analysis have been provided in the Supplementary Information (SI).
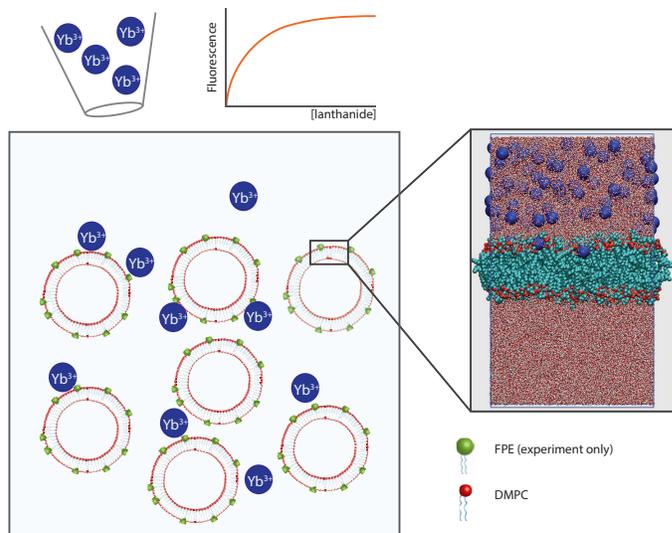
Fig. 1 (Left) Sketch of the experimental set up. On top, a pipette filled with Yb^{3+}, represented using dark blue circles, adds increasing concentrations of $YbCl_3$ to a solution containing vesicles of DMPC. Some DMPC lipid are replaced by fluoresceinphosphatidylethanolamine (FPE) (green circles in the bilayer). (Right) Snapshot of the molecular dynamics model mimicking the experimental set up. Blue spheres – Yb^{3+}, cyan sphere – aliphatic chains, red spheres in bilayer – oxygen atoms in phosphate group. Water is represented with red and white small spheres.

Molecular Dynamics simulations of a DMPC bilayer in an aqueous solution of ytterbium chloride were performed using a combi-

nation of force-fields: GROMOS 43A1-S3[34] for the lipids, OPLS-AA parameters as starting point to model the short range interactions for the Yb^{3+} and Cl^- ions,[35] and the SPC/E model for water.[36] SPC/E provides a good prediction of the dielectric constant of water, and it has been used extensively in the simulation of aqueous solutions and interfaces. We note that the combination of GROMOS 43A1-S3 and OPLS-AA parameters is not commonly used in computer simulations. However, we have shown that it can, in combination with the SPC/E model, accurately predict the coordination number of Yb^{3+}. For this force-field parameters the coordination number, 8, was found to be in good agreement with the experiment.[37] The force-fields employed to model the DMPC bilayer (see Supplementary Information) predict structural properties (see results section below), such as area per lipid, thickness and aliphatic chain order parameters that are in good agreement with previous simulation and experimental data.[38]

To simulate the systems represented in Fig. 1, and take into account the presence of salt in one leaflet of the bilayer, we performed our simulations under confinement conditions. Far from the bilayer we set two soft "walls", which kept the solution in one region of the simulation box (see Fig. 1 and the SI for further details). We performed simulations in the presence and absence of salt, and in the case of pure water we performed additional computations with full periodic simulation boxes, in order to test the validity of our "wall" approach. We find that the "wall" approach predicts properties in good agreement with a full periodic system.

A typical simulation consisted of a DMPC bilayer of 400 lipids, 10 Yb^{3+} cations plus the corresponding, Cl^-, counterions, and over 5×10^4 water molecules per leaflet. This corresponds to a water:lipid ratio of 140:1, which is above the excess water point of DMPC (31-36:1 water:lipid molecules) for temperatures in the range 298-323 K.[39] The simulations were performed in the isothermal-isobaric ensemble, and the electrostatic interactions in the two dimensional system were computed using a corrected three dimensional Ewald method.[40] The equations of motion were integrated with a timestep of 2 fs using the leap-frog algorithm and the parallel code GROMACS4.5.[41] The simulation trajectories were analysed to calculate the area per lipid, bilayer thickness, ion-lipid coordination, interdigitation coefficients and deuterium order parameters. Details on the approaches used to obtain these quantities are explained in detail in the SI.

3 Results and discussion

Our experimental ^{1}H NMR results demonstrating the effects of lanthanide addition to DMPC extruded vesicles as a function of temperature are shown in Fig. 2 and Fig. 3 (See SI for more details). Phospholipids are known to exhibit characteristic ^{1}H NMR peaks.[42] In the present investigation we focus on the peaks resulting from the protons in the "head group" and in the aliphatic "chain-region" as labelled in Fig. 2. Lanthanides are known to cause a chemical shift change and peak broadening and quenching when added to phospholipid moieties. The magnitudes of these are defined by the effects on electron and nuclear spin relaxation which lead to line broadening and chemical shift changes respectively.[43] The addition of Yb^{3+} induces a positive change (towards 0 ppm) in the chemical shift whilst Dy^{3+} induces an
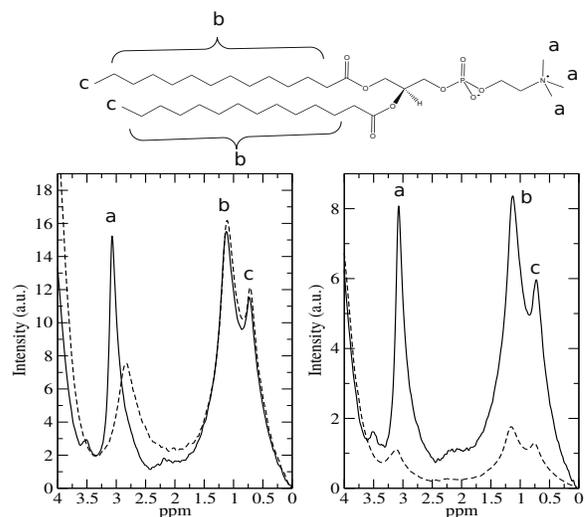
Fig. 2 (Top) DMPC structure including labelling of the principal hydrogens, a is N-methyl headgroup, b is chain methylenes and c are terminal methyl protons. (Bottom) Example MAS-^{1}H NMR traces for (left) DMPC only (solid), 0.025 Yb^{3+}:DMPC ratio(dashed)), (right) DMPC only (solid), 0.002 Dy^{3+}:DMPC ratio(dashed) at 321K.

opposite effect due to the positive and negative magnetic susceptibility of Yb^{3+} and Dy^{3+} ions respectively.[44,45] These changes are observed in the example spectra shown in Fig. 2 and quantified in Fig. 3.

Previous NMR studies of lipid-vesicle interactions with lanthanide ions have reported differences between the inner and outer lipid head group signals upon addition of lanthanide ions. An example of this is a ^{31}P-NMR study looking at the addition of Pr^{3+} to DMPC/5-DOXYL sub 100 nanometer spin labelled liposomes, where splitting of the resonances depends strongly on pH and Pr^{3+} concentration.[46] Notably, the studies that report these differences were performed using vesicles formed via sonication. This technique results in vesicles with diameters of the order of 10's of nanometers. These systems are highly curved and therefore, the interpretation of the lanthanide:lipid interaction should consider both curvature and lanthanide:lipid effects. In our case, extruded 100 nm phospholipid vesicles were used to minimise curvature effects and therefore we do not resolve the differing head group signals. The effects of curvature and the differing inner and outer head group signals are the subject of a separate investigation.

The addition of Yb^{3+} and Dy^{3+} to DMPC vesicles induces positive and negative chemical shifts (δppm) respectively. These differences are attributed to the different magnetic susceptibilities. Above the gel to fluid transition temperature there is little change in the chemical shift where the mean δppm is -0.04 $\pm$ 0.02 for the Dy^{3+} system and 0.26 $\pm$ 0.03 for the Yb^{3+} system between 298 and 333 K. This behaviour has been previously reported in the chemical shifts of lipid head groups observed in vesicles of Egg PC and DPPC upon the external addition of 6 mM Pr^{3+} above the gel to fluid transition temperatures.[5] Above the gel transition temperature there is a significant increased mobility within the

acyl chain region which is reflected in the motion of the lipid head groups.[47] Model membrane systems are impermeable to lanthanide ions, as supported by the simulation data described in later sections, which detected no lanthanides crossing the bilayer. This study therefore focuses on the bilayer-lanthanide surface interactions quantified via the quenching of the N-methyl lipid head group signal. The NMR data shows no change in line width for the terminal methyl and methylene chain protons (Fig. 2, top, labelled b and c) upon the addition of $YbCl_3$ above the phase transition temperature. Interestingly there is a quenching effect in both the terminal methyl and methylene chain protons upon the addition of $DyCl_3$ above the phase transition temperature. One possible explanation for this difference is that Dy^{3+} has a larger magnetic moment (Dy:10.65 vs Yb:4.54) causing pseudocontact interactions effects on the lipid hydrocarbon chain region inside the bilayer.[48] This implies that $YbCl_3$ is more suitable for surface interaction studies and hence the focus on $YbCl_3$ for the simulation studies.
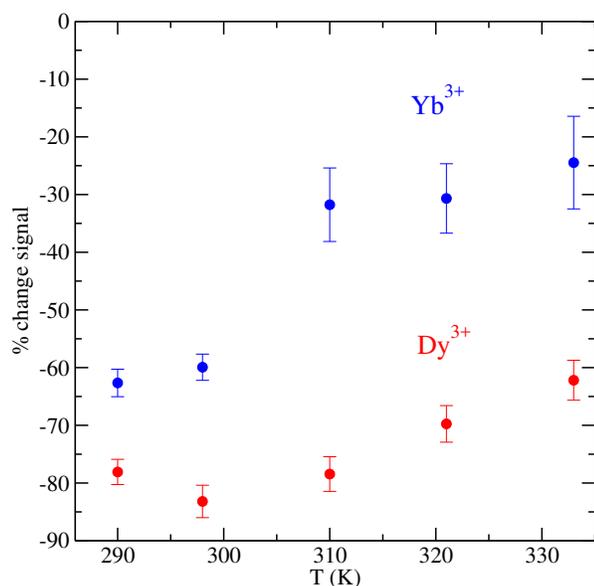
Fig. 3 Effects of lanthanide addition to DMPC vesicles as a function of temperature showing changes in quenching of the N-Methyl lipid head group ^{1}H NMR signal.

Broadening and quenching of the N-methyl lipid head group signal relative to the vesicles with no lanthanides, was noted in both cases as shown in Fig. 2 and Fig. 3. Dy^{3+} showed a larger quenching effect in comparison to Yb^{3+} despite the smaller number of Ln^{3+} ions present due to the presence of 5 unpaired electrons compared to the 1 unpaired electron in Yb^{3+}. The changes in quenching of the N-methyl lipid head group signal upon the addition of lanthanide ions have been quantified in Fig. 3 relative to the pure vesicular system. These were calculated using OriginLab data analysis software to fit normalised NMR data, where the chemical shift was defined as the peak centre and the quenching calculated from the percentage reduction in peak area. The procedure for this calculation has been explained in detail in the Supplementary Information. A reduction in quenching was observed for both Yb^{3+} and Dy^{3+} ions (Fig. 3) with increasing

temperature, implying a possible temperature association of the lanthanide:lipid molecular interaction. This was more prominent for Yb^{3+} than Dy^{3+}. Previous work[45] has shown a temperature dependence with lanthanide association where normalised alkyl chain order parameters have been shown to decrease with increasing temperature (303-343 K) for the addition of Tm^{3+} to DMPC/DHPC bicelles. Increasing concentrations of Tm^{3+} enhanced the order parameters at any given temperature. Notably this included a phase transition from the bicelle positively aligned nematic phase to a smectic phase coexisting with an isotropic phase at a temperature influenced by the lipid to lanthanide ratio (higher Tm^{3+}, lower temperature).[45] Our basic NMR characterisation of lanthanide and DMPC interactions have shown good agreement with previous literature and therefore support the additional experiments and molecular mechanisms described below.
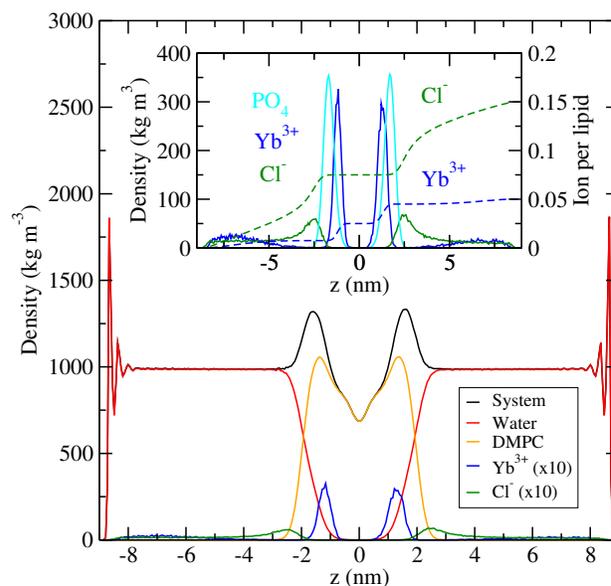
Fig. 4 (Main Plot) Density profiles (kg m^{-3}) of System A at 323K and 1 bar. Density profiles of the DMPC bilayer-solution system: total (black line), water (red line), DMPC membrane (orange), ytterbium (blue) and chloride (green). Notice that the density of the ions has been increased by a factor of ten. (Inset) Ion and phosphate group density profiles. The dashed line represents the running integral of the ytterbium and chloride density profiles. All the properties are calculated with reference to the centre of mass of the membrane.

Fig. 4 shows the simulated density profiles of the DMPC bilayer, upon addition of 10 $YbCl_3$ per leaflet. The data were obtained following a lengthy equilibration, $\sim 0.4 \, \mu s$, to allow for ion adsorption.[16] All the simulations reported below correspond to a temperature of 323 K and a normal pressure of 1 bar. The oscillations at -8 < z < 8 nm are induced by the confining walls. We tested that the presence of the walls did not influence the interaction of the ions with the bilayers. Indeed, the properties obtained with this method are consistent with the ones calculated with full periodic simulation boxes. A comparison of the two methods is given below. The ionic density profiles feature a strong peak at the surface of the DMPC bilayer. The chloride density reaches a maximum at a position that corresponds well with the location of the positively charged choline group, which defines the most

external region of the membrane. The Yb^{3+} cation, penetrates more deeply into the bilayer, and it binds to the lipids on the plane defined by the negatively charged phosphate groups (see Fig 4). Our computational calculations of the electrostatic potential across the membrane lump together the dipole and surface electrostatic potential, which are well distinguished in the experiments.[49] Thus, the simulation values are higher than the wet experimental study. In Fig. 5, we show the computational results. The electrostatic potential across the membrane is -0.36 V in the case of the System B, which involves a high salt Yb^{3+}:lipid ratio of 0.25. This potential shift is induced by the ions located on the right hand side of the membrane. The ion and charge density profiles (see Fig. 4 and 6) features the characteristic electric double layer structure. The charge density, and the ensuing electrostatic field, is significant and decays in a relatively long length-scale, of the order of the membrane thickness (~ 4 nm). (see Fig. 6). The build up of charge at the bilayer induces a positive shift in the electrostatic potential of the membrane. The electrostatic potential increases by ~ 110 mV in going from pure water to $YbCl_3$ (0.025 $YbCl_3$:lipid ratio). This increase is consistent with previous computational studies of other salts where shifts of ~ 85-100 mV were reported upon addition of NaCl to DPPC bilayers[28,50,51] Therefore, our membrane (dipole) potential is within the accepted range obtained in simulations with classical non-polarizable forcefields. Differences between the experimental and simulation electrostatic potentials, in particular the so called dipole potential, have been discussed in Ref. 52.
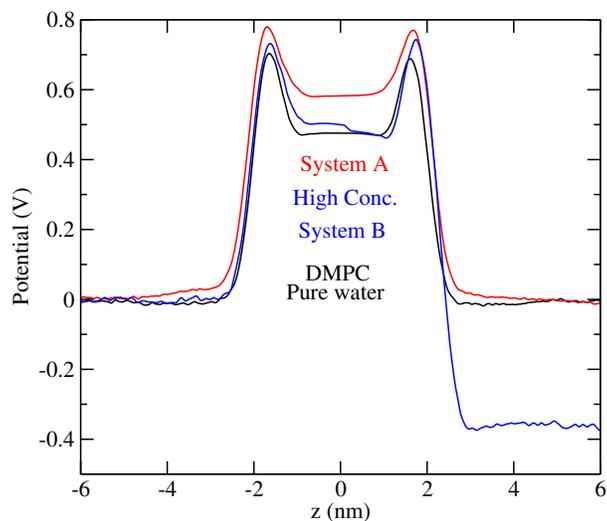
Fig. 5 Electrostatic potential of the bilayer at 323K and 1 bar as a function of ytterbium:lipid ratio: no salt (black line), intermediate Yb^{3+}:lipid ratio (0.025) with salt on both sides of the bilayer (red line), and high salt content Yb^{3+}:lipid ratio (0.25) with salt on the side (z>0) of the bilayer (right,blue line).

Experimentally, we have carried out pyranine leakage assays to corroborate the presence of the electric double layer observed in the simulations. Briefly, this experiment involved inducing a sudden pH gradient across a DMPC pyranine loaded vesicle either in the presence or absence of lanthanide ions. This led to a leakage of protons across the bilayer and then a change in inter vesicu-
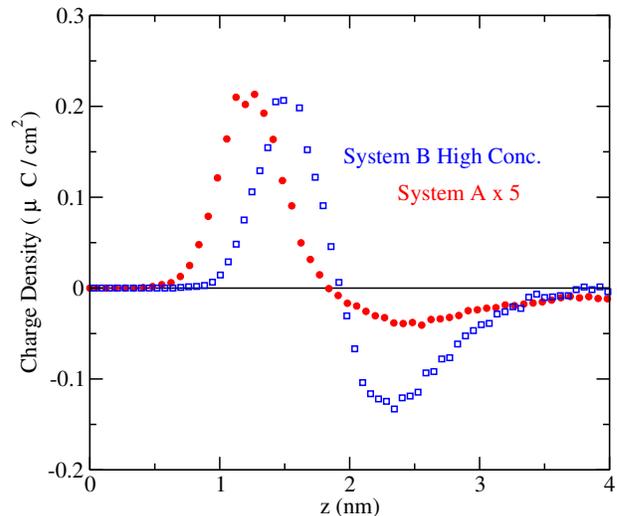
Fig. 6 Total ionic charge density along the direction perpendicular to the bilayer plane. $z = 0$ corresponds to the centre of mass of the membrane. The data for System A (red points) correspond to the lower Yb^{3+}:lipid ratio (0.025), and have been multiplied by 5 to allow a direct comparison with the System B (blue points), which corresponds to the higher Yb^{3+}:lipid ratio (0.25) of the saturated state.

lar pH characterised by a decrease in fluorescence. In Fig. 7, we have reported a biphasic change in fluorescence after the addition of an external acidic pH gradient to DMPC vesicles loaded with pyranine. After addition of 1M HCl and 98.4 mM $YbCl_3$ in 1 M HCl, an immediate change is seen in the fluorescence followed by a subsequent slower decrease to zero fluorescence. Within the uncertainty of our method, no change in fluorescence occurs in the absence of a pH gradient across the vesicle membrane. It is expected that some binding of pyranine to the DMPC membrane occurs, however this is prior to the addition of the pH gradient in the presence or absence of lanthanides and hence it would not influence the differences in fluorescence noted. Lipid vesicles are stable under pH gradients and impermeable to encapsulated pyranine, hence fluorescence changes are not attributed to pyranine leakage or vesicle instability.[53] Previous investigations have also reported biphasic changes in fluorescence upon the application of a pH gradient across asolectin phospholipid membranes.[54,55] More recently this has been modelled in POPC vesicles in the presence and absence of the ion channel gramicidin.[56] These have been attributed to an initial rapid efflux of protons across the vesicle membrane, inducing a transmembrane electrical potential which leads to a second counterion limited proton-counterion exchange. Notably there is a significant difference in the initial rapid fluorescence change when the pH gradient is induced in the presence of lanthanides ($YbCl_3$). This effect could be attributed to the electrostatic double layer of observed in simulations, and the adsorption of the cations in the membrane surface. The electric double layer and the associated electrostatic field would reduce the initial rapid efflux of protons across the membrane, leading to the initial smaller change in fluorescence that we observe experimentally.

To shed more light into the nature of the electric double layer, we estimated the ratio lipid:Yb^{3+} by integrating the simulated

System	YbCl$_3$:lipid ratio	Area (nm^2)	Thickness (nm)	λ_{id} (nm)	K_a (mN/m)
YbCl$_3$/DMPC/YbCl$_3$ (System A)	0.025	0.608(0.002)	3.39(0.05)	0.53(0.04)	763(14)[a]
YbCl$_3$/DMPC/H$_2$O (System B)	0.025	0.624(0.006)	3.34(0.02)	0.56(0.01)	—
YbCl$_3$/DMPC/H$_2$O (System B)	0.25	0.605(0.003)	3.38(0.08)	0.54(0.05)	—
H$_2$O/DMPC/H$_2$O (2-walls)	0	0.637(0.007)	3.32(0.07)	0.54(0.03)	—
H$_2$O/DMPC/H$_2$O (no-walls)	0	0.639(0.005)	3.31(0.03)	0.55(0.08)	290(6)
H$_2$O/DMPC/H$_2$O (Exp.[38])	0	0.633	3.52	—	234(23)[b]

Table 1 Bilayers simulated in this work. All the simulations were performed at 323 K and 1 bar and for different Yb^{3+}:lipid ratios. We present data for the YbCl$_3$:lipid ratio, area per lipid (Area), bilayer thickness, interdigitation coefficient, and area compressibility modulus. In parenthesis represent the standard deviation of associated to the data. [a] This simulations were performed using two bilayers (as suggested in Ref. 50) and full periodic boundary conditions.; [b] Experimental data at 302 K from Ref. 57.
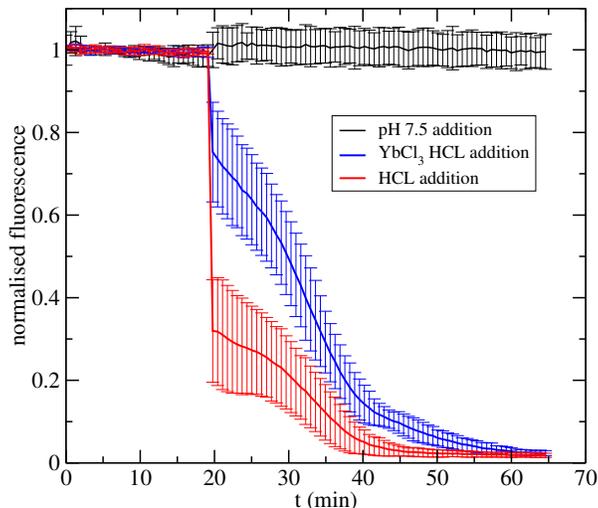
Fig. 7 Proton leakage assays showing fluorescence changes in pyranine loaded DMPC extruded vesicles under constant conditions, a pH gradient induced via the external addition of HCl and an identical pH gradient induced in the presence of YbCl$_3$ ions. Proton leakage across the DMPC membrane reduces the intravesicular pH and leads to a decrease in pyranine fluorescence.

Fig. 8 Radial distribution function of ytterbium with atoms of water and lipids, within a cutoff distance of 0.8 nm. The dark green solid lines represent interactions with the atoms in the *sn-1* tail. The red solid lines are the radial distributions functions of the atoms in the *sn-2* tail, the core of the glycerol structure are the light green solid lines, the blue solid lines are the phosphate groups, the choline atoms are represented by the black solid lines, and the atoms of water are the cyan solid lines. The inset represents in logarithmic scale, the radial distribution functions for a Yb-atom cutoff of 0.4 nm. The lines follow the same matching between colours and parts of the lipid. The peaks with the closest atoms to Yb cation have been highlight using numbers (see structure plotted into the graph), both in the graph and the lipid structure.

Yb^{3+} density profiles. The running integral (see Fig. 4) shows that the ratio Yb^{3+}:lipid is 0.025 (see Table 1 for numerical data). The density profiles for Yb^{3+} and Cl$^-$ are zero in the interior of the bilayer which indicates the absence of ion exchange between the upper and lower leaflets for our simulation time scales, $\sim$0.4 μs. The ytterbium binds strongly to the membrane and our density profiles (see plateau between main peak and bulk) do also indicate that lack of ion exchange between the bilayer and the solution at sub-microsecond time scales. To further analyse the Yb^{3+}-DMPC interactions we computed the radial distribution function (RDF) of the ytterbium ions with lipids and water. Fig. 8 shows the RDFs of Yb^{3+} cations absorbed in the membrane. A cutoff of 0.4 nm was employed to identify the nearest neighbours of the Yb^{3+} cations (see inset of Fig. 8).

The first coordination shell of Yb^{3+} consists of oxygens that can be divided in two main groups. Firstly, oxygens belonging to water molecules, $r \sim 0.23$ nm, and secondly oxygens that are part of the phosphate group in the DMPC lipids. The integration of the oxygen(water) peak indicates that the cation is surrounded by 7-8 water molecules (not as nearest neighbours, see Fig. 8).

Indeed, a simulation snapshot reveals that the ions can drag significant water well within the head group region (see Fig. 9-top and Fig. 9-bottom). These molecules are also part of the solvation shell of the phosphate group. In the inset of Fig. 8, the peak at 0.31 nm corresponds to the hydrogens bonded to the water molecules. The position of the peaks is compatible with a configuration where the water dipoles point radially away from the Yb-O vector.

The oxygen peaks around 0.22 nm in Fig. 8, corresponds to the oxygens in the phosphate group and in the carbonyl group of the *sn-2* tail, which are the first neighbours of the Yb^{3+} when this is located at the bilayer. Note that the oxygens of the *sn-1* chain are not directly interacting with Yb^{3+} ions (see the inset of RDFs in Fig. 8, which only involve *sn-2* oxygens), since these kind of oxygens are deeper than the *sn-2*, this situation confirms the results reported in Ref. 58 for a DMPC bilayer having NaCl. Our radial

distribution functions for Yb^{3+} show similar features to those reported by Cormodi *et al.* [16] for other cations: Li^+, Na^+, K^+, Mg^{2+}, Ca^{2+}, Sr^{2+}, Ba^{2+}, and Ac^{3+}. By using our RDFs we are able to study the lipid binding around the cation. It shows a clear preference for the lipids to interact with the cation via carbonyl and phosphate oxygens, which is consistent with the results reported in previous works. [10,16,19,20,22]

We used the radial distribution function to calculate the cation-lipid coordination. The results were obtained from the analysis of trajectories spanning 100 ns. For Yb^{3+}:lipid ratios relevant to NMR experiments, the Yb^{3+} cations are strongly coordinated to 5 lipids, as nearest neighbours. The coordination numbers are shown to vary little (within the uncertainty of our computations) with temperature: 5.15, 5.13, and 4.75 for 298 K, 310 K, and 323 K, respectively. The overall coordination of the Yb^{3+} cation
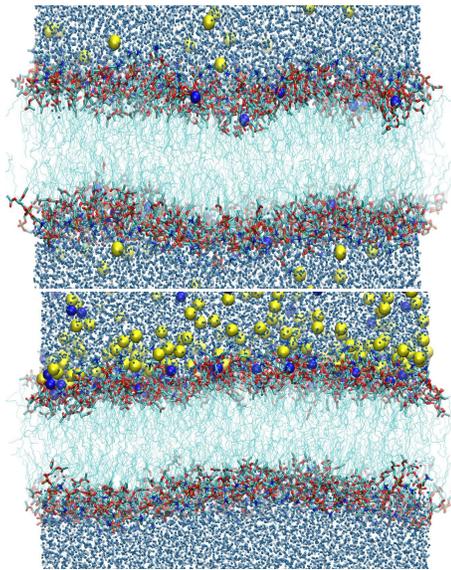
Fig. 9 (Top) Snapshot of System A at the lower Yb^{3+}:lipid ratio (0.025). and (Bottom) Snapshot of System B at high Yb^{3+}:lipid ratio (0.25). The snapshots illustrate the Yb^{3+} position into the membrane for both systems. Blue and yellow spheres represent the cations and anions, respectively. The head groups have been represented with thick bonds and the corresponding aliphatic chains with thin bonds. The oxygen atoms in the water molecules are represented with small blue spheres.

corresponds to 7 nearest neighbours with a water:lipid ratio of 2:5. Hence, the adsorption of the cation in the bilayer requires a strong dehydration of Yb^{3+}, with respect the water coordination in bulk water, 8, which is in good agreement with the experimental estimates. [37] The dehydration is favoured by a strong coordination of the cation with the lipids. We show in Fig. 9 two snapshots illustrating the equilibrium position of Yb^{3+} and Cl^- ions into the membrane, both in the System A and System B at high Yb^{3+}:lipid ratio. The simulations indicate that ytterbium penetrates well in the polar region of the lipids and it interacts both with the lipid as well as with water.

We have focused so far on the coordination of the Yb^{3+} cation with the lipids and water. We discuss in the following the impact that the salt has on the area per lipid, the bilayer width and the conformation of the aliphatic chains. Table 1 compiles the sim-

ulated structural properties for the different systems investigated here. We performed additional simulations of bilayers containing pure water, using both the standard full periodic boundary condition approach and our "walls" method. We found that both methods (see Fig. 2 of SI) produced equivalent results.

We report in Table 1 the area per lipid for the different systems investigated in this work. Our results for systems without salt show good agreement with available experiments [38] and other computational studies, [8,16] confirming the accuracy of our force-fields. The simulations indicate that the addition of salt results in a slight decrease, $\sim 5\%$, of the area per lipid (c.f. Systems A and "2-walls" in Table 1). This reduction is consistent with previous computer simulations of POPC bilayers in NaCl solutions. [16,59] We have also examined the impact that the asymmetric distribution of salt, employed in the vesicle experiments, has on the area per lipid. Our simulations show that the areas per lipid of the symmetric and asymmetric system are very similar (c.f. System A and System B). The asymmetry induces a small increase in the area per lipid, of the order of $\sim 2\%$. The results presented above show that the area per lipid changes little upon addition of salt, despite the strong Yb^{3+}:lipid interaction revealed by the radial distribution functions (see Fig. 8). We have further quantified the structural changes of the membrane by evaluating the thickness, and interdigitation coefficient. The latter measures the overlap of the two lipid leaflets. These quantities also feature small deviations with respect to salt free bilayers. As an additional test, we investigated the influence of salt on the structure of the aliphatic chains, by computing the "deuterium" order parameter. The order parameter obtained from simulations in absence of salt shows very good agreement with existing experiments of DMPC bilayers at 323 K. [60] $YbCl_3$ increase the order parameter, S_{CD} (see Fig 10), both for the *sn1* and *sn2* chains (labelled as 'b' in Fig. 2), which would be compatible with a higher packing of the lipids, as reflected in the decrease of the area per lipid (see Table 1).

We have shown above that the membrane thickness changes little, possibly suggesting a small change in the conformation of the lipids, to accommodate the increased ordering of the aliphatic chains. However, one would expect significant changes in the configuration of the head groups, since the Yb^{3+} binds strongly to the phosphates (see Fig. 8). To test this idea we computed the head group tilt angle, θ, for two systems: pure (no salt) DMPC and System A with salt:lipid ratios similar to those used in the NMR experiments (see Table 2). We define the tilt angle as the angle between the P-N vector and the normal vector of the membrane. We have considered separately the angles for both upper and lower leaflets (u, l), in order to differentiate the impact of the salt on the asymmetric systems. The average tilt angle for the reference system (pure water) is similar to those reported before for DMPC bilayers, [61] $\sim 78^o$. The addition of salt induces a significant reduction of the head group angle, becoming more aligned with the bilayer normal (c.f. "System A" and "2-walls" in Table 2). Such changes in the head group conformation have been correlated before with an increase in the electrostatic potential of the bilayer membrane, which is consistent with the +ve 110 mV shift induced by the Yb salt (see Fig. 5).

The noticeable change in the tilt angles of the Phosphate group,
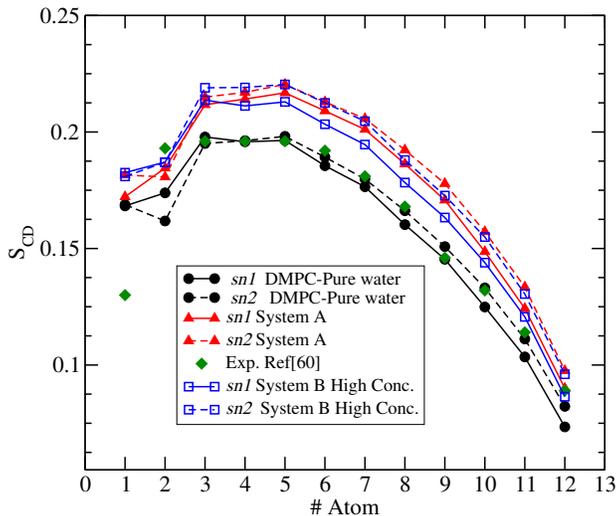
Fig. 10 Simulated "deuterium" order parameter, S_{CD} of the aliphatic chains. Black lines represent salt free conditions, System A with intermediate salt, Yb^{3+}:lipid ratio 0.025 (red lines) and System B with high salt ratio Yb^{3+}:lipid ratio 0.25 (blue). sn1 and sn-2 contributions are represented with full and dotted lines, respectively. The simulation results are compared with experimental data of a DMPC bilayer (salt free conditions) for the sn-2 chain only, and at 323 K.[60]

prompted us to investigate the impact of $YbCl_3$ on the mechanical properties of DMPC. We computed the area compressibility modulus using the fluctuation route (see SI for simulation details). Table 1 compiles our values for free salt and $YbCl_3$ bilayers. Our results for free salt conditions, ~ 290 mN/m, show good agreement with previous studies, both experimental results[57], ~ 234 mN/m, and simulation values,[62], ~ 334 mN/m. The salt is found to increase significantly, more than double ~ 760 mN/m, the area compressibility modulus of DMPC.

System	YbCl:lipid ratio	θ_u	θ_l
System A	0.025	69.83(0.03)	69.20(0.03)
System B	0.25	52.86(0.02)	78.63(0.02)
2-walls	0	78.05(0.07)	77.72(0.07)

Table 2 Head group angle (in degrees) with the vector normal to the bilayer plane as a function of salt Yb^{3+}:lipid ratio. θ_u and θ_l represent the tilt angles of the upper lower leaflets, respectively. For System B only the upper leaflet is in contact with the salt. The values in parenthesis represent the error associated to the data.

To complete our investigation we have carried out additional assays of association of lanthanides and lipids in the fluorescence based FPE labelled vesicles. Briefly, the association was determined by fitting the fluorescence data shown in Fig. 11 to a Hill model and calculating the lanthanide concentration at the 90% saturation point of the fluorescent signal. This was then converted to a ratio by dividing half the total number of lipids in the experiment by the absolute number of lanthanide ions at the 90% saturation point. This was performed for three independently prepared samples, each of which was measured 3 times. In Fig. 12, the points reflect the mean and standard error of the independent
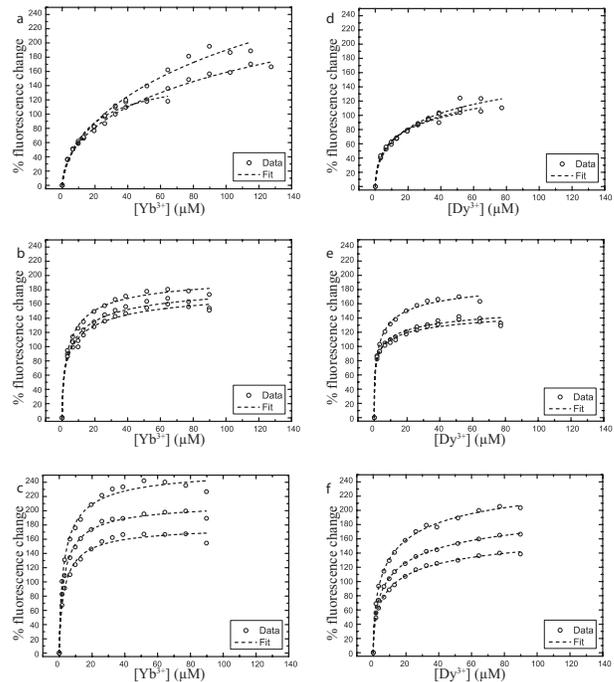
Fig. 11 Results showing % fluorescence change for titration of lanthanide solutions into FPE-labelled extruded DMPC vesicles at a) Yb^{3+} 298 K, b) Yb^{3+} 310 K, c) Yb^{3+} 321 K, d) Dy^{3+} 298 K, e) Dy^{3+} 310 K, f) Dy^{3+} 321 K. Each data set indicates an independent experiment.

experiments.

The saturated concentrations at different temperatures are collected in Table 3.

T(K)	$[Yb^{3+}]$ (μM)	$[Dy^{3+}]$ (μM)
298	218	1632
310	200	835
321	51	607

Table 3 Saturated concentrations for Yb^{3+} and Dy^{3+} at different temperatures. Concentrations are given in μM.

At 298 K, which is 2 K above the gel-fluid transition temperature for DMPC, 90% saturation occurred at a Yb^{3+}:lipid ratio of 0.88 ± 0.09 for Yb^{3+} and 0.13 ± 0.06 for Dy^{3+} (see Fig. 12). This increased to 1.11 ± 0.34 and 0.49 ± 0.33 for Yb^{3+} and Dy^{3+} respectively at 310 K and 3.70 ± 0.26 and 0.30 ± 0.04 at 321 K. The Ln^{3+}:lipid saturation is constant within the errors at 298 K and 310 K but increases at 321 K, in the Yb^{3+} sample although a small increase is seen in comparison to the 290 K value for Dy^{3+}. Higher temperatures will increase lipid mobility and diffusion of lanthanide ions. Lanthanides have previously been shown to interact with the phospholipid head group region.[6,63] An increased head group mobility would enable a greater number of lanthanide ions to interact. This may have less of an impact on Dy^{3+} in comparison to Yb^{3+} due to size differences.

The NMR analysis shows some distinctive changes in the chemical shifts and quenching of the N-methyl lipid head groups, which point towards a significant adsorption of the lanthanides at the
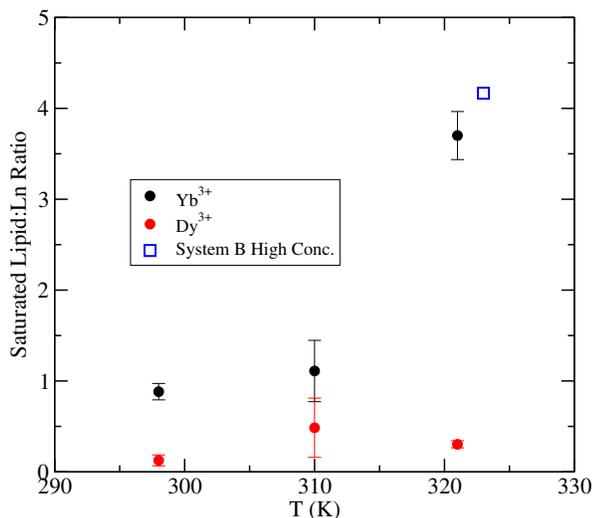
Fig. 12 Lipid:lanthanide ratio at 90% of fluorescence signal saturation from titration experiments, calculated from Hill fits of the data as described in the main text. The black points are the values of Yb^{3+}, the red points are Dy^{3+} results and the open square represents the simulated state discussed in the text, corresponding to the high concentration of Yb^{3+}.

surface of the vesicle. Strong adsorption is also supported by the large ratio of lipid:Ln^{3+} that we infer from our fluorescence experiments. The ability of membranes to adsorb high quantities of Yb^{3+} is surprising. The possibility of a high stoichiometry Lipid:cation has been noted before,[64] although these early estimates relied on the use of the Gouy-Chapman theory. This theory however did not provide a good fitting of experiments involving DPPC and Lanthanides.[64] Hence the coordination of the lanthanides in the saturated state requires further study. Motivated by this, we performed additional simulations of a concentrated solution of $YbCl_3$. We considered the asymmetric salt system to match the experiments performed with vesicles. The simulations show that the structure of the bilayer is maintained, even at this high Yb^{3+}:lipid ratio, 0.25. We show in Fig. 9-Bottom a snapshot of the equilibrated bilayer at high salt:lipid ratio corresponding to saturation conditions. The snapshot shows a clear preference for the ions to adsorb on a plane defined by the head group. Stronger accumulation of Cl^- is also evident. This is reflected in a strong electric double layer as revealed by the charge density in Fig. 6, with a concomitant increase of the electrostatic potential of $\sim$ 367 mV. Again, the strong ion adsorption in the saturated system, has little impact on the average structural properties; area per lipid, membrane thickness or interdigitation (see Table 1). The "deuterium" order parameter is similar to the one obtained at lower salt:lipid ratios (see Fig. 10). However the head group tilt angle decreases substantially, $\sim$ 30 % with respect to the pure bilayer (c.f. "System B" and "2-walls" in Table 2). The change in the head group orientation is driven by the electrostatic environment generated by the ytterbium adsorption in the DMPC bilayer.

We performed additional simulations of the saturated system, to test whether we could see pore formation. These simulations spanned 200 ns. We did not find evidence for pore formation nor Yb^{3+} translocation. We note that pore formation can be observed

relatively quickly, $\sim$ 5 ns, in computer simulations when there is charge asymmetry which leads to net electrostatic fields.[31] Hence, we expect the time scale investigated here is long enough to address the possible nucleation of pores. Unlike charge asymmetric systems, our simulations and experiments involve "salt" asymmetry instead, which does not lead to a permanent electrostatic field across the bilayer. Hence we conclude that asymmetry in salt concentration is not enough to induce pore formation. Our computer simulations support the experimental assumption that the Yb^{3+}:lipid ratios commonly used in experimental studies do not lead to ion translocation.

4 Conclusions

In this paper we have investigated the interactions between Lanthanides and DMPC bilayers using NMR, fluorescence and computer simulations. We focused our simulations on $YbCl_3$ solutions, which are commonly used in NMR experiments to calculate lipid flip-flop rates.

The simulations show that the ytterbium cations bind strongly to the bilayer, hence supporting the experimental conclusions. The environment of the ytterbium cation in the membrane is defined by 7 nearest neighbours, with a water:lipid ration of 2:5. The binding of the ytterbium to the oxygen atoms in the phosphate group allows the strong dehydration of the cation when it moves from solution to the bilayer environment. The strong ion adsorption gives rise to an electrostatic double layer, and to a positive shift ($+ve \sim 110$ mV) of the electrostatic potential of the bilayer, with respect to the electrostatic potential of the free-salt membrane. The presence of the electric double layer is consistent with the results obtained from experiments of pyranine leakage assay, which demonstrate that the protonic leak across the membrane slows down drastically when lanthanide ions are adsorbed in the membrane. We thus conclude that the electrostatic potential arising from ion adsorption can block the pathways for proton transfer across the membrane.

Ytterbium salt does not lead to large changes in the average structural properties of the bilayer, namely, area per lipid, membrane thickness or membrane interdigitation. Since the interaction with the lipid is mainly via the lipid head groups, which are distinct from the lipid tails, this could explain how despite a strong cation:membrane interaction, there are no changes in these structural properties. The simulated "deuterium" parameter reveals a slight increase in the ordering of the aliphatic chains. These conclusions apply to the saturated state too, which corresponds to a high ytterbium to lipid ratio, 1:2-4, as inferred from our assays on the association of lanthanides and lipids performed in fluorescent FPE labelled vesicles. However, $YbCl_3$ modifies significantly the orientation of the phosphate head group relative to the bilayer plane. The lipids adopt a more vertical orientation with respect to the free salt case. This conformational change is consistent with the increase in the membrane electrostatic potential, and it facilitates the accommodation of the lanthanide ions in the head group region. We also find that the membrane stiffness increases significantly upon addition of $YbCl_3$. At concentrations relevant to NMR experiments, the area compressibility modulus increases by a factor of 2.6 with respect to the free-salt mem-

brane. This increment is similar to the effect of that cholesterol of on biological membrane (see Ref. 65). Previous experimental work of DPPG membranes in the presence of NaCl[66], also reported a strong dependence of the area compressibility modulus with ionic strength. In that case, the screening of the lipid charges upon addition of salt made the membrane more elastic (lower area compressibility modulus), showing that electrostatic interactions do indeed induce a stiffening of the membrane. Our results are consistent with these observation, since the membranes considered here are neutral, and they become charged upon addition of $YbCl_3$, hence a stiffening would be expected.

We conclude that lanthanides interact strongly with biological membranes. Despite this DMPC membranes preserves their main structural properties, even at lanthanide:lipid ratios corresponding to ion saturation conditions. The simulations support the experimental perception that addition of Yb^{3+} does not lead to ion translocation nor pore formation. The modifications in the membrane electrostatic potential, head group orientation and membrane elasticity must however be taken into account in the estimation of flip-flop rates. This problem will be addressed in a future publication.

5 Acknowledgments

References

1 B. Alberts, A. Johnson, J. Lewis, M. Raff, K. Roberts, and P. Walter, *Molecular Biology of the Cell*, Garland Science, 2002.

2 J. Wall, C. A. Golding, M. V. Veen, and P. O'Shea, *Mol. Membr. Biol.*, 1995, **12**(2), 183–192.

3 J. L. Richens, J. S. Lane, M. L. Mather, and P. O'Shea, *J. Colloid Interface Sci.*, 2015, **457**, 225–231.

4 C. H. Evans, *Biochemistry of the Lanthanides*, Springer US, Boston, MA, 1990.

5 G. Royden, A. Hunt, and L. R. Tipping, jan , 1980, **12**(1), 17–36.

6 R. E. Joyce, T. L. Williams, L. C. Serpell, and I. J. Day, *Chem. Phys. Lett.*, 2016, **648**, 124–129.

7 G. van Meer, D. R. Voelker, and G. W. Feigenson, *Nat. Rev. Mol. Cell Biol.*, 2008, **9**(2), 112–124.

8 A. P. Lyubartsev and A. L. Rabinovich, *Biochim. Biophys. Acta - Biomembr.*, 2016, **1858**(10), 2483–2497.

9 H. I. Ingólfsson, M. N. Melo, F. J. V. Eerden, C. Arnarez, C. A. López, T. A. Wassenaar, X. Periole, A. H. D. Vries, D. P. Tieleman, and S. J. Marrink, *J. Am. Chem. Soc.*, 2014, **136**, 14554–14559.

10 P. Mukhopadhyay, L. Monticelli, and D. P. Tieleman, *Biophys. J.*, 2004, **86**(3), 1601–1609.

11 S. a. Pandit, M. L. Berkowitz, P. Mukhopadhyay, L. Monticelli, D. P. Tieleman, S. a. Pandit, D. Bostick, and M. L. Berkowitz, *Biophys. J.*, 2002, **82**(4), 1818–1827.

12 S. a. Pandit, D. Bostick, and M. L. Berkowitz, *J. Chem. Phys.*, 2003, **119**(4), 2199–2205.

13 S. a. Pandit, D. Bostick, and M. L. Berkowitz, *Biophys. J.*, 2003, **84**(6), 3743–3750.

14 R. A. Böckmann, A. Hac, T. Heimburg, and H. Grubmüller, sep , 2003, **85**(3), 1647–1655.

15 R. A. Böckmann and H. Grubmüller, *Angew. Chemie - Int. Ed.*, 2004, **43**(8), 1021–1024.

16 A. Cordomí, O. Edholm, and J. J. Perez, feb , 2008, **112**(5), 1397–1408.

17 A. a. Gurtovenko and I. Vattulainen, *J. Phys. Chem. B*, 2009, **113**(20), 7194–7198.

18 S. J. Marrink, A. H. de Vries, and D. P. Tieleman, *Biochim. Biophys. Acta - Biomembr.*, 2009, **1788**(1), 149–168.

19 M. Stepniewski, A. Bunker, M. Pasenkiewicz-Gierula, M. Karttunen, and T. Rog, *J. Phys. Chem. B*, 2010, **114**(36), 11784–11792.

20 R. Vácha, P. Jurkiewicz, M. Petrov, M. L. Berkowitz, R. A. Böckmann, J. Barucha-Kraszewska, M. Hof, and P. Jungwirth, *J. Phys. Chem. B*, 2010, **114**(29), 9504–9509.

21 A. A. Gurtovenko, J. Anwar, and I. Vattulainen, oct , 2010, **110**(10), 6077–6103.

22 M. Pasenkiewicz-Gierula, K. Baczynski, M. Markiewicz, and K. Murzyn, oct , 2016, **1858**(10), 2305–2321.

23 B. Qiao and M. Olvera de la Cruz, oct , 2013, **4**(19), 3233–3237.

24 B. F. Qiao and M. Olvera de la Cruz, may , 2013, **117**(17), 5073–5080.

25 H. L. Tepper and G. a. Voth, *Biophys. J.*, 2005, **88**(5), 3095–108.

26 H. L. Tepper and G. A. Voth, oct , 2006, **110**(42), 21327–37.

27 S. J. Marrink, F. Jähnig, and H. J. Berendsen, *Biophys. J.*, 1996, **71**(August), 632–647.

28 S. K. Kandasamy and R. G. Larson, *J. Chem. Phys.*, 2006, **125**(7), 074901.

29 H. Leontiadou, A. Mark, and S. Marrink, *Biophys. J.*, 2007, **92**(12), 4209–4215.

30 A. A. Gurtovenko and I. Vattulainen, *Biophys. J.*, 2007, **92**(6), 1878–1890.

31 A. a. Gurtovenko and I. Vattulainen, *J. Phys. Chem. B*, 2007, **111**(48), 13554–13559.

32 P. W. Nolden and T. Ackermann, *Biophys. Chem.*, 1976, **4**(3), 297–304.

33 M. Kaszuba and G. Hunt, *J. Inorg. Biochem.*, 1990, **40**(3), 217–225.

34 S.-W. W. Chiu, S. a. Pandit, H. L. Scott, and E. Jakobsson, mar , 2009, **113**(9), 2748–2763.

35 C. Cossy, A. C. Barnes, J. E. Enderby, and A. E. Merbach, *J. Chem. Phys.*, 1989, **90**(6), 3254.

36 H. J. C. Berendsen, J. R. Grigera, and T. P. Straatsma, *J. Phys. Chem.*, 1987, **91**, 6269–6271.

37 L. Helm, F. Foglia, T. Kowall, and A. E. Merbach, jun , 1994, **6**(23A), A137–A140.

38 N. Kucerka, M. P. Nieh, and J. Katsaras, *Biochim. Biophys. Acta - Biomembr.*, 2011, **1808**(11), 2761–2771.

39 S. C. Costigan, P. J. Booth, and R. H. Templer, *Biochim. Biophys. Acta - Biomembr.*, 2000, **1468**(1-2), 41–54.

40 U. Essmann, L. Perera, M. L. Berkowitz, T. Darden, H. Lee, and L. G. Pedersen, *J. Chem. Phys.*, 1995, **103**, 8577–8593.

41 B. Hess, C. Kutzner, D. van der Spoel, and E. Lindahl, *J. Chem. Theory Comput.*, 2008, **4**, 435–447.

42 M. L. Sparling, R. Zidovetzki, L. Muller, and S. I. Chan, apr , 1989, **178**(1), 67–76.

43 T. Moriya, apr , 1963, **18**(4), 516–520.

44 S. H. Park, C. Loudet, F. M. Marassi, E. J. Dufourc, and S. J. Opella, *J. Magn. Reson.*, 2008, **193**(1), 133–138.

45 R. S. Prosser, J. S. Hwang, and R. R. Vold, may , 1998, **74**(May), 2405–2418.

46 W. W. Sulkowski, D. Pentak, K. Nowak, and A. Sulkowska, *J. Mol. Struct.*, 2006, **792-793**, 257–264.

47 G. Hunt and L. R. Tipping, feb , 1978, **507**(2), 242–261.

48 R. L. Carlin in *Magnetochemistry;* Springer Berlin Heidelberg, Berlin, Heidelberg, 1986; chapter 9, pp. 237–261.

49 P. O'Shea, oct , 2003, **31**(5), 990–996.

50 A. A. Gurtovenko and I. Vattulainen, *J. Am. Chem. Soc.*, 2005, **127**(50), 17570–17571.

51 D. Robinson, N. A. Besley, P. O'shea, and J. D. Hirst, *J. Comput. Chem.*, 2011, **32**(12), 2613–2618.

52 L. Wang, *Annu. Rev. Biochem.*, 2012, **81**(1), 615–635.

53 R. M. Straubinger, D. Papahadjopoulos, and K. Hong, *Biochemistry*, 1990, **29**(20), 4929–4939.

54 N. R. Clement and J. M. Gould, *Biochemistry*, 1981, **20**, 1534–1538.

55 P. S. O'Shea, S. Feuerstein-Thelen, and A. Azzi, jun , 1984, **220**(3), 795–801.

56 M. Megens, C. E. Korman, C. M. Ajo-Franklin, and D. A. Horsley, *Biochim. Biophys. Acta - Biomembr.*, 2014, **1838**(10), 2420–2424.

57 W. Rawicz, K. C. Olbrich, T. McIntosh, D. Needham, and E. Evans, *Biophys. J.*, 2000, **79**(1), 328–339.

58 A. A. Gurtovenko, *J. Chem. Phys.*, 2005, **122**(24), 1–10.

59 A. Lervik, F. Bresme, and S. Kjelstrup, *Phys. Chem. Chem. Phys.*, 2012, **14**(10), 3543–53.

60 J. P. Douliez, a. Léonard, and E. J. Dufourc, *Biophys. J.*, 1995, **68**(May), 1727–1739.

61 C.-J. Högberg and A. P. Lyubartsev, jan , 2008, **94**(2), 525–531.

62 Q. Waheed and O. Edholm, *Biophys. J.*, 2009, **97**(10), 2754–2760.

63 M. Petersheim, H. Halladay, and J. Blodnieks, sep , 1989, **56**(3), 551–557.

64 H. Akutsu and J. Seelig, *Biochemistry*, 1981, **20**(26), 7366–7373.

65 E. Evans and D. Needham, jul , 1987, **91**(16), 4219–4228.

66 B.-S. Lu, S. P. Gupta, M. Belička, R. Podgornik, and G. Pabst, *Langmuir*, 2016, **32**(50), 13546–13555.